

EUVL resist based aberration metrology

Germain L. Fenger¹, Sudharshanan Raghunathan², Lei Sun², Obert R. Wood², and Bruce W. Smith¹

¹Rochester Institute of Technology, 168 Lomb Memorial Dr, Rochester, NY 14623, USA

²GLOBALFOUNDRIES, 257 Fuller Rd, Albany, NY 12203, USA

ABSTRACT

Extreme Ultraviolet Lithography (EUVL) at 13.5 nm is currently the most promising technology for advanced integrated circuit (IC) manufacturing nodes. Since the wavelength for EUVL is an order of magnitude smaller than current optical lithography systems (193 nm), wavelength scaled tolerances on lens manufacturing must be tightened to avoid image distortion and contrast loss as these scale with wavelength. Therefore understanding the aberrations of an EUVL system both in idle and production conditions is paramount. This study aims to assess a photoresist based technique for capturing pupil information of EUVL systems that can be implemented during full system use. Several data sets have been collected on an ASML EUV Alpha-Demo Tool (ADT) using the latest Center for Nanoscale Science and Engineering (CNSE) baseline resist Shin-Etsu SEVR139. Various one-dimensional and two-dimensional binary structures were imaged and used for pupil extraction in conjunction with computational modeling and simulations. Results show a stable extracted aberration signature over several measurements. Results also show that the method is sensitive to sub-nm levels of aberration change.

1. INTRODUCTION

Lens aberrations directly impact the image fidelity of a lithographic process [1]. Modern lithographic systems require tight tolerances on all sources of error and require precise and accurate methods to determine system aberration levels. The pupil function of such an aberrated system is shown in equation (1.1), where $H(r,\theta)$ is the aperture function, and $W(r,\theta)$ is the wavefront aberration function, both shown in polar coordinates. The wavefront aberration function is typically described by Zernike polynomials, composed of normalized coefficients orthogonal over a unit circle [2,3].

$$P(r, \theta) = H(r, \theta) \exp \left[i \frac{2\pi}{\lambda} W(r, \theta) \right] \quad (1.1)$$

Interferometry methods are highly accurate ways to perform aberration measurements on single optical elements and full lithographic systems, including tests such as knife-edge test [4], point-diffraction interferometry [5], phase-shifting point-diffraction interferometry [6,7], and shearing interferometry [8]. While these tests provide highly accurate measurements, they are difficult to carry out during photolithography system use as they require the integration of a sensor efficient at the exposure wavelength and suitable for high resolution measurements.

Extreme ultraviolet lithography (EUVL) is faced with many challenges. One of those challenges is the measurement and monitoring of aberrations at the sub-nm level. EUVL will require that the total RMS of the wavefront be in the range of 30 milliwaves (equivalent to 0.41 nm) [9], making sensitive aberration metrology methods important. The stability of aberration levels during full system use has not been investigated to a significant extent for source power scaled to production levels. Simulations have been conducted to show that reticle heating can be managed using appropriate cooling methods [10], however it will be crucial to have in-situ wavefront aberration monitoring that is compatible with full system use to verify aberration stability until EUVL becomes as mature as previous generation lithographic tools. An in-situ and independent method of wavefront aberration monitoring is therefore beneficial. Well characterized photoresist image methods can be employed, which rely on targets that are sensitive to a particular aberration. These methods have been investigated in the past for DUV lithography [11–13] and a similar approach is used here for EUV lithography. Figure 1 shows several targets that are commonly used for such aberration tests. These features include phase edges and dots [14–16], alternating phase shift mask (PSM), five bar structures, DRAM isolation pattern, and line

width in various orientations [11]. These structures are often coupled with variations in illumination shape, numerical aperture (NA), exposure dose, focus, and variations in target critical dimension (CD) [12,14,15,17] to give more degrees of freedom and the ability to predict higher order aberrations with a unique solution.

Binary Mask Structure	{CD ver} - {CD hor}	{CD left} - {CD right}	{CD left} - {CD right}	CD Through Pitch
Aberration Sensitivity	Astigmatism	Coma/Trefoil	Trefoil/Coma	Spherical
Phase Mask Structure	Phase edge shape/ CD	Phase edge shape/ CD	FEM Tilt/ Delta CD	Defect Printing
Aberration Sensitivity	All	All	Coma/ Spherical	All

Figure 1: Various binary and phase structures that can be used to determine aberration levels in an optical system. The square outlines showing the CD measurement location for the targets used in this study.

Using print based methods in a partial coherent system causes some unavoidable pupil averaging, reducing the effects of aberrations on printed images, and while this may be beneficial to manufacturing integrated circuits, for the purposes of this experiment it is not ideal. For example, Figure 2 shows the image placement error caused by 40 mλ of coma of an isolated space. As partial coherence is increased there is more averaging in the pupil wavefront and less image shift is seen.

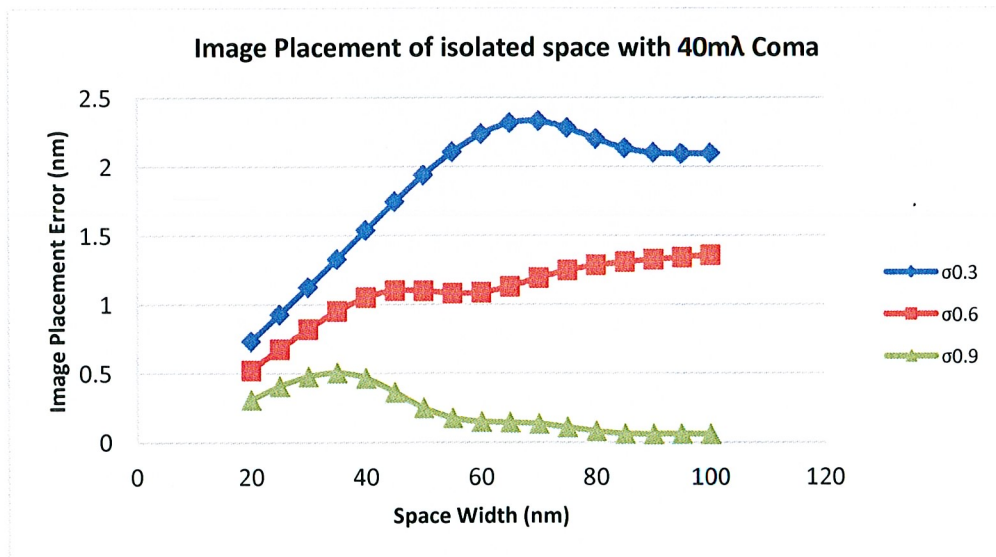


Figure 2: Image placement error of an isolated space imaged with the presence of 40 mλ coma (NA 0.25, λ 13.5 nm)

2. EXPERIMENT

The study initially limits the parameters of the experiment to currently available EUVL tools. The primary tool used in this investigation was an ASML Alpha Demo Tool (ADT) at the Center for Nanoscale Science and Engineering (CNSE) at the University of Albany, NY. The system has a numerical aperture (NA) of 0.25 and partial coherence (σ) of 0.5. Resist based tests are ideally carried out with a highly coherent source (low σ) to decrease diffraction order spread and increase sensitivity. The relatively large value of partial coherence of the system limited fitting to lower aberration order. Target structures were chosen based on the diffraction interaction in the pupil. The structure must interact with the area of the pupil that the desired aberration effects. The binary structures that were used include 1:1 lines through pitch of various orientations, five bar, and DRAM isolation structures. Several exposures of features found on existing reticles were completed through dose and focus. Resist CD measurements were then taken with a Hitachi CD4000 scanning electron microscope (SEM). This CD data was then added as input into a custom optimization software program that interfaces with a lithography simulator (PROLITH™ v14.0.3.1). The software program, which is described below, fits predictive models to simulated scenarios of a wide range of aberrated wavefronts. Using these models and the resist CD data, a wavefront was fit and a particular set of Zernike coefficients were used to describe said wavefront. Because the system under test has a fixed partial coherence of 0.5, the targets were only able to probe for and fit low order aberrations, with higher order aberrations averaged into the extracted aberration value. The aberrations that were extracted include primary astigmatism (Z_5 & Z_6), coma (Z_7 & Z_8), spherical (Z_9), trefoil (Z_{10} & Z_{11}). A full scalar model was used for the simulations. The simulator was interfaced with MATLAB™ and automated, running approximately ~20,000 simulations for a typical fitting set.

2.1 Modeling & Extraction

The first step in the flow described in Figure 3 is to fit astigmatism and coma concurrently. For astigmatism two models were created that use the CD difference of 1:1 lines, with a typical pitch of 90 nm, in vertical and horizontal orientations for astigmatism x and 45° and 135° for astigmatism y through focus. The sensitivity of the models was found to be 0.075nm Δ CD/m λ astigmatism. The model was also verified to be robust through simulations with added noise from other primary aberrations up to 80m λ . Using these models, initial values for astigmatism x and y were determined. Concurrently, models were fit and used to find the initial value of coma x and y. The models for coma use a 5 bar structure in orthogonal orientations with a typical pitch of 64nm 1:1. The impact of coma aberration is evaluated by measuring the CD difference between the 1st and 5th bar. The sensitivity of the model was similarly found to be 0.075 nm Δ CD/m λ coma. The five-bar structure is also significantly sensitive to trefoil with a sensitivity of 0.015nm Δ CD/m λ trefoil. The model was also verified to be robust with added noise from other aberrations up to 80 m λ non-coma and trefoil primary aberrations. After initial values for coma and astigmatism were obtained, primary spherical aberration was fit. Spherical fitting required more data than coma and astigmatism and is fit by measuring the best focus shift through pitch. This requires a focus exposure matrix (FEM) for each pitch. Figure 4 shows the change in best focus (delta) response for various spherical aberration levels through pitch values from 64 to 256 nm and a line CD of 32 nm. Using the initial values for astigmatism and coma in the FEM, this method was used to determine an initial value for spherical aberration using a best fit for all pitch values. Once astigmatism, coma, and spherical have initial solutions, trefoil was then fit. Using the previous solutions, a model for trefoil was created using the left-right CD difference from a DRAM isolation pillars with a vertical pitch of 128 nm, horizontal pitch of 240 nm and CD of 160 by 32 nm. The model was fit at best dose for different trefoil values and used to obtain an initial value for trefoil x and y; trefoil y uses the same structure rotated 90°. The sensitivity of the model was found to be 0.070 nm Δ CD/m λ trefoil. Table 1 shows a summary of the test structures described as well as the test output. The next part of the flow as seen in Figure 3 was iterating through model building and fitting using existing values for Zernike coefficients and the extraction of new Zernike coefficients.

Once initial values of primary aberrations were determined, new models were created by simulating the pertinent Zernike coefficient effect on the CD metric or focus shift for aberrations up to Z_{11} . This process was iterated using the previous iteration Zernike coefficient values as input for the new model. This was done until the Zernike coefficients were stable and changed less than 5% for each coefficient. Then the output wavefront was displayed together with the determined coefficient values. An example wavefront is shown in the next section.

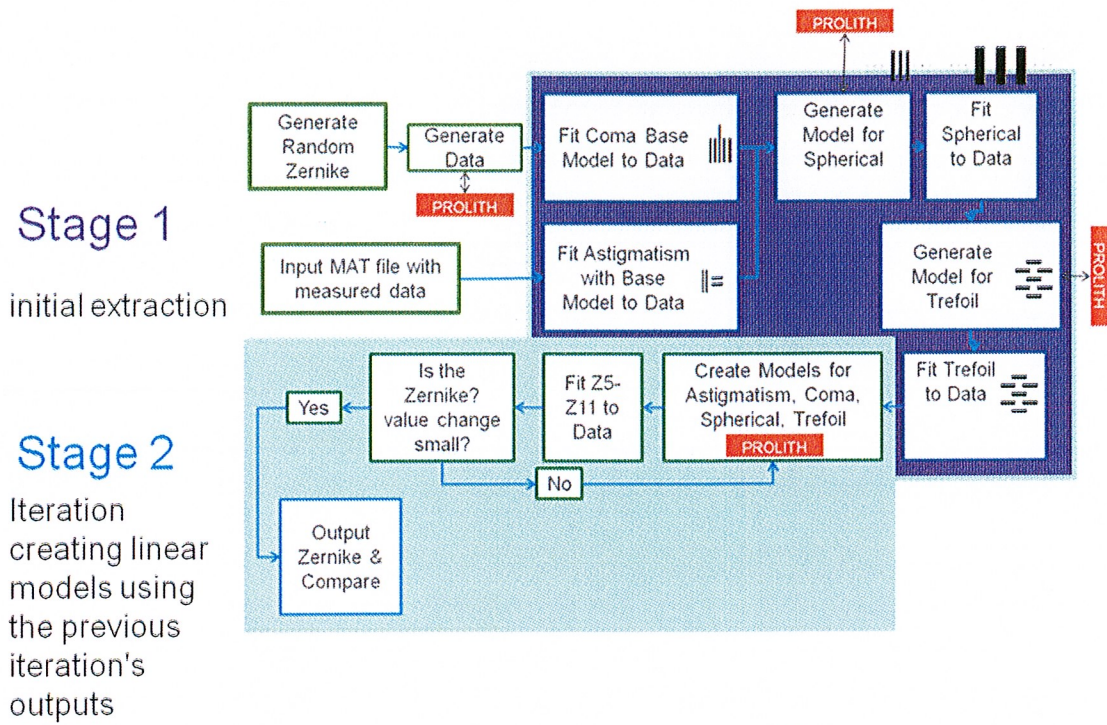


Figure 3: Extraction flow used in aberration fitting using MATLAB™ and PROLITH™

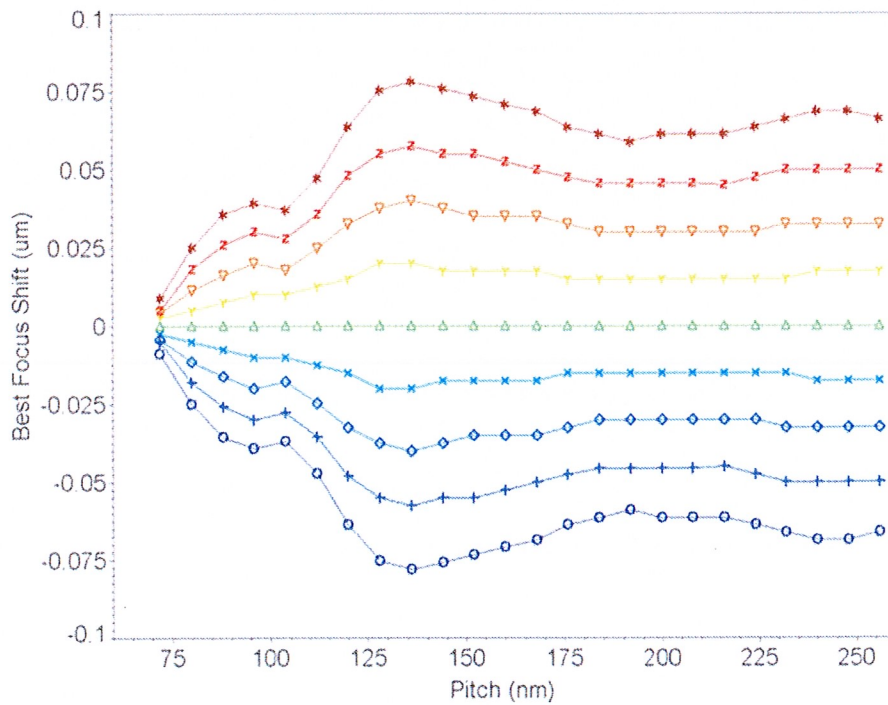


Figure 4: Simulation of expected best focus shift through pitch for a range of spherical aberration levels for the ADT

Table 1: Binary structures found to be sensitive for the ADT

Aberration	Z5	Z6	Z7	Z8	Z9	Z10	Z11
Binary test Structure	Horizontal and vertical lines CD: 45nm 1:1	45° and 135° lines CD: 45nm 1:1	Vertical 5 bar structure CD: 32nm 1:1	Horizontal 5 bar structure CD: 32nm 1:1	Horizontal lines through pitch (60nm-260nm) CD:32nm	Horizontal brick wall structure V-pitch: 128nm H-Pitch: 240nm V-CD: 32nm H-CD: 160nm	Vertical brick wall structure V-pitch: 240nm H-Pitch: 128nm V-CD: 160nm H-CD: 32nm
Test Output	Horizontal and vertical line CD difference through focus	45° and 135° line CD difference through focus	Left and right bar CD difference through dose	Top and bottom bar CD difference through dose	Best focus through pitch	Left and right CD difference through dose	Top and bottom CD difference through dose

2.2 Target selection and data collection

Targets were selected for experimental investigation that were both sensitive to the aberration and available for the system under test. Table 2 shows the structures that were used. Because the method described in the previous section is flexible and input parameters can be modified as needed, similar structures can be substituted for a given target.

Table 2: Binary structures used for experimental validation on the ADT

<i>Aberration</i>	<i>Function</i>	<i>Binary test Structure</i>	<i>Test Output</i>
Z_5 astigmatism x	$\sqrt{6} \rho^2 \cos 2\theta$	Horizontal and vertical lines CD 40nm 1:1	Horizontal and vertical line CD difference through focus (bright field)
Z_6 astigmatism y	$\sqrt{8} \rho^3 \sin 3\theta$	45° and 135° lines CD: 40nm 1:1	45° and 135° line CD difference through focus (bright field)
Z_7 coma x	$(3\rho^3 - 2\rho) \cos \theta$	Vertical five bar structure CD: 35nm 1:1	1st and fifth bar CD difference (bright field)
Z_8 coma y	$(3\rho^3 - 2\rho) \sin \theta$	Horizontal five bar structure CD: 35nm 1:1	1st and fifth bar CD difference (bright field)
Z_9 primary spherical	$6\rho^4 - 6\rho^2 + 1$	Horizontal lines through pitch P64-192nm CD:32nm	Best focus through pitch (bright field)
Z_{10} trefoil x	$\rho^3 \cos 3\theta$	Horizontal T-bar structure V-pitch: 120nm H-Pitch:300nm V-CD: 30nm H-CD: 210nm	Left and right CD difference (bright field)
Z_{11} trefoil y	$\rho^3 \sin 3\theta$	Vertical T-Bar structure V-pitch: 120nm H-Pitch:300nm V-CD: 30nm H-CD: 210nm	Top and bottom CD (bright field)

For each dataset, three resist-coated wafers were exposed on the EUV ADT; structures are repeated 8 times per field and 21 fields per wafer. The resist used for the experiments is 75 nm SEVR139 on silicon wafers.

A focus meander was first carried out, centered at best focus and having 21 steps of 20 nm. The CD of P80 lines in four orientations were measured to extract astigmatism. The change in the difference in CD per focus was fit to simulations to give an effective astigmatism value. Figure 5 shows an example of P80 nm SEM images used in the astigmatism x fitting. There were 192 measurements for astigmatism x and the same for astigmatism y on the first wafer.

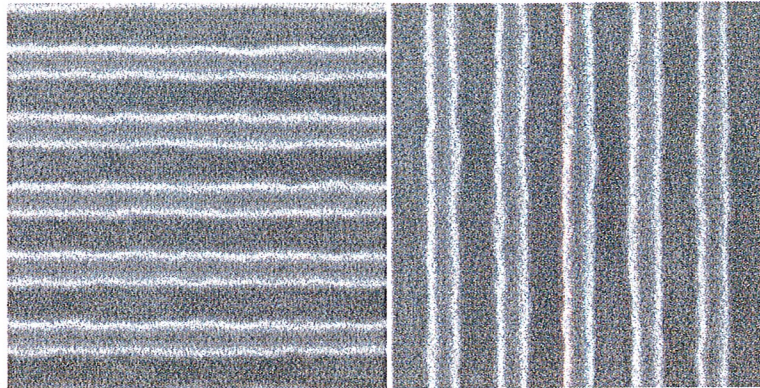


Figure 5: P80 horizontal and vertical lines used to extract astigmatism x

The second exposed wafer consisted of an exposure series having 21 dies and was used for extraction of coma and trefoil. Being even aberrations, they are not sensitive to focus variations. For the extraction of coma the 1st and the 5th bar of a five bar structure were measured, as shown in Figure 6. The difference in CD was fit to simulations and an effective coma value was determined. Similarly, trefoil was fit to the CD difference of the ends of a T-bar structure shown in Figure 7.

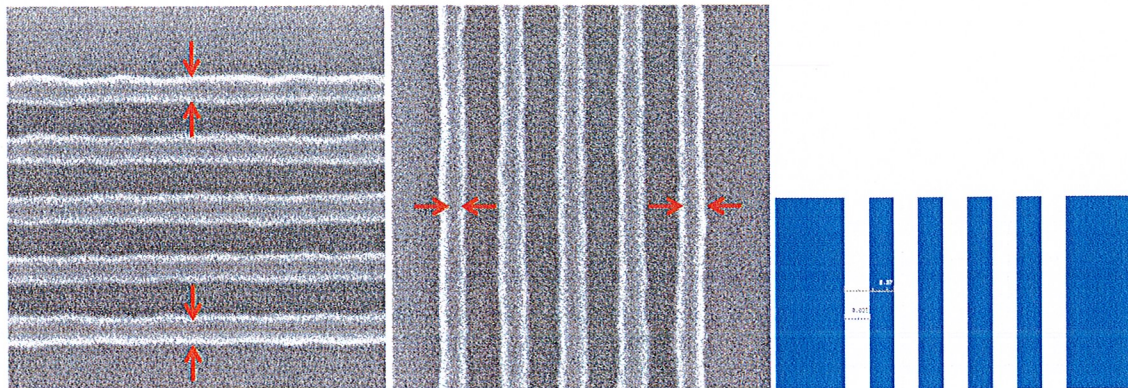


Figure 6: (Left) SEM image of five bar structures used in the extraction of coma (Right) Bright field five bar design

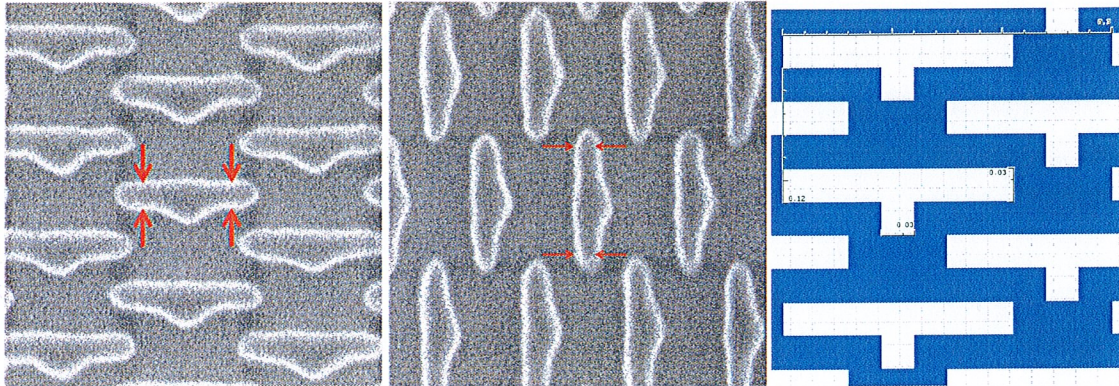


Figure 7: (Left) SEM image of T-Bar structures used in the extraction of trefoil. (Right) Dark field design of T-Bar structure

The third exposed wafer was a focus exposure matrix (FEM) to determine best focus for several different pitches. The best focus was taken as the focus value where the through focus behavior is symmetric around that point. Figure 8 shows example SEM images of the five pitches that are measured, P64, P96, P128, P160, and P192.

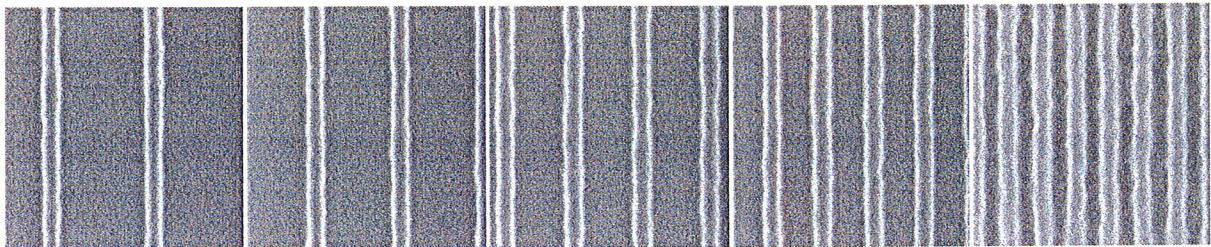


Figure 8: SEM images of P192 – P64 nm

The three wafers needed for a complete data set were exposed on the same day, or within a few days to minimize tool variations. Once data collection from the three wafers was complete, the measured values and experimental settings were fed into the fitting program. The next section will go in more detail about the fitting process as well as go over the results.

2.3 Aberration fitting and experimental results

The CD-SEM data was formatted into one input file, which was loaded in the fitting program. Using lithography simulation, a model was created for the expected CD differences or focus shifts due to aberration. Then the experimental data was fit for a certain aberration level. This process of creating models and fitting data was repeated, forward feeding the aberration results to the next iteration. Figure 9 shows the graphical user interface (GUI) of the aberration fitting program and an example output of the fit pupil, Zernike coefficients and x and y cross-sections of the pupil.

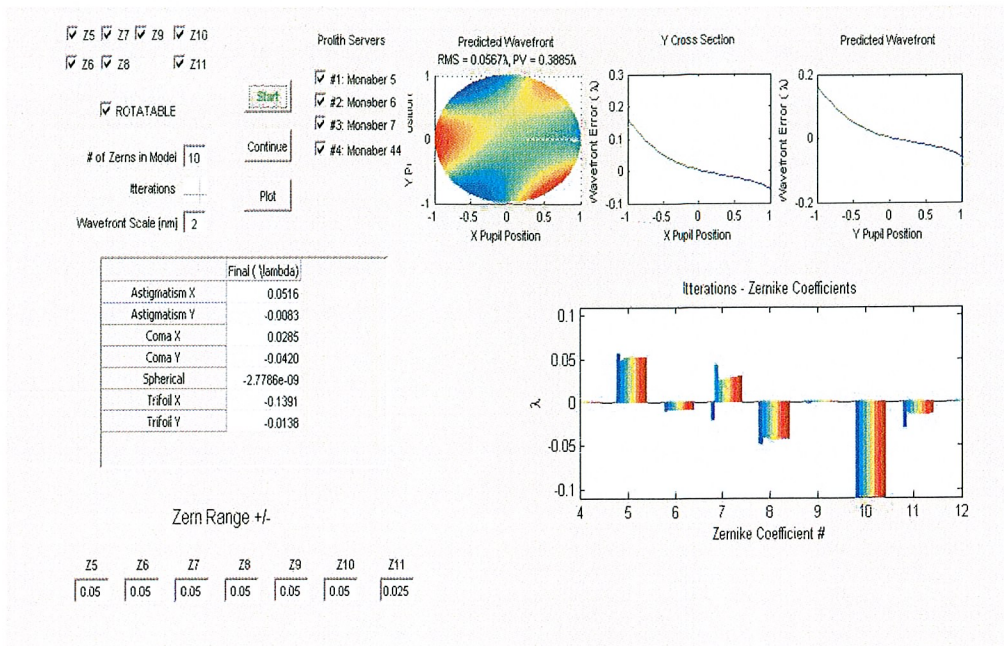


Figure 9: GUI for the aberration fitting program, showing an example output

Four datasets were collected to determine the repeatability of this method. Datasets A and B were at standard conditions measured approximately one month apart. Dataset C was taken after a major repair of the system in standard conditions to see if the tool had drifted after the maintenance. Dataset D, taken immediately after dataset C, was taken after the machine constants were altered to increase astigmatism x by $\sim 50 \text{ m}\lambda$, to show the sensitivity of the method. Figure 10 shows the extracted aberration results of the 4 datasets. The largest aberration consistently found on the tool was trefoil x (Z_{10}). The datasets seem to be in reasonable agreement of the aberration signature of the tool. Also dataset D, with the increase of astigmatism x by $\sim 50 \text{ m}\lambda$, shows a definite increase in the extracted value, with a difference from dataset C of $72 \text{ m}\lambda$.

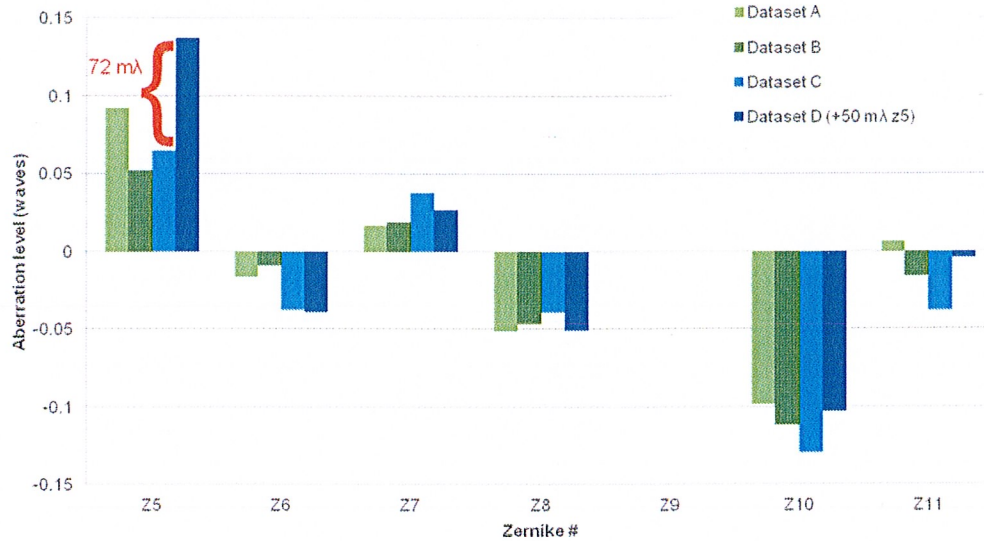


Figure 10: Graph of Zernike coefficients output of the 4 collected datasets from the ADT

3. CONCLUSION

The complementary method to traditional approaches of determining and monitoring aberrations in EUVL systems has been shown. Image based aberration monitoring has a unique opportunity in EUVL. Due to tighter lens tolerances in absolute wavefront distortion and potential negative effects from heating, it may be necessary to monitor aberration levels during system use, something that is not possible using traditional methods. The absolute sensitivity of the presented method scales with wavelength and in terms of wavelength, wavefront distortion tolerances in EUVL compared to DUV (193 nm) lithography are much more relaxed, making an image based approach applicable for EUVL.

The presented method used one-dimensional and two-dimensional binary structures imaged in a partially coherent EUVL system in conjunction with computational modeling and simulation. It was successfully shown that the image based method can be used to monitor an aberration signature composed of primary as well as some higher order aberrations up to Z_{11} . The datasets were collected using three wafer exposures of specific test targets selected for the ASML alpha demo tool. It is believed that these three wafers can be further reduced to one wafer for periodic monitoring. It was also shown that the method is repeatable and sensitive to aberration change with a detection of an induced ~ 50 mλ change in astigmatism x , measuring 72 mλ.

4. ACKNOWLEDGMENTS

The author would like to especially thank Lena Zavyalova for her insight and many valuable discussions, Luke Orsini for help with exposures, KLA Tencor for the use of PROLITH™, the U.S. Department of Education Graduate Assistance in Areas of National Need (GAAN) program and the Semiconductor Research Corporation (SRC/GRC) for their support. This work was performed by the Research Alliance Teams at various IBM research and development facilities.

5. REFERENCES

- [1] B. W. Smith and R. E. Schlieff, "Understanding lens aberration and influences to lithographic imaging," *Proceedings of SPIE* **4000**, 294–306 (2000) [doi:doi:10.1117/12.389018].
- [2] B. Smith, "Optics for Photolithography," in *Microlithography*, K. Suzuki and B. Smith, Eds., pp. 149–242, CRC Press (2007).

- [3] von F. Zernike, "Beugungstheorie des schneidenverfahrens und seiner verbesserten form, der phasenkontrastmethode," *Physica* **1**, 689–704 (1934) [doi:10.1016/S0031-8914(34)80259-5].
- [4] L. Foucault, "Description des procedes employes pour reconnaitre la configuration des surfaces optiques," *C. R. Acad. Sci.* **47**, 958ff (1858).
- [5] W. P. Linnik, "A simple interferometer for the investigation of optical systems," *Proc. Academy of Sci. of the USSR* **1**, 208 (1933).
- [6] H. Meddecki, E. Tejnil, K. A. Goldberg, and J. Bokor, "Phase-shifting point diffraction interferometer," *Opt. Lett.* **21**, 1526 (1996) [doi:10.1364/OL.21.001526].
- [7] P. Venkataraman and B. W. Smith, "Aberrations of steppers using phase-shifting point diffraction interferometry," *Proceedings of SPIE* **4000**, 1245–1249 (2000) [doi:doi:10.1117/12.388962].
- [8] P. P. Naulleau, K. A. Goldberg, and J. Bokor, "Extreme ultraviolet carrier-frequency shearing interferometry of a lithographic four-mirror optical system," *J. Vac. Sci. Technol. B* **18**, 2939 (2000) [doi:10.1116/1.1321290].
- [9] C. G. Krautschik, M. Ito, I. Nishiyama, and T. Mori, "Quantifying EUV imaging tolerances for the 70-, 50-, 35-nm modes through rigorous aerial image simulations," *Proceedings of SPIE* **4343**, 524–534 (2001) [doi:doi:10.1117/12.436684].
- [10] A. Abdo, B. La Fontaine, and R. Engelstad, "Predicting the thermomechanical distortion of extreme ultraviolet lithography reticles for preproduction and production exposure tools," *J. Vac. Sci. Technol. B* **21**, 3037 (2003) [doi:10.1116/1.1619955].
- [11] K. van Ingen Schenau, H. Bakker, M. Zellenrath, R. Moerman, J. Linders, T. Rohe, and W. Emer, "System qualification and optimization for imaging performance on the 0.80-NA 248-nm step-and-scan systems," *Proceedings of SPIE* **4691**, 637–651 (2002) [doi:doi:10.1117/12.474612].
- [12] J. P. Kirk, "Review of photoresist-based lens evaluation methods," *Proceedings of SPIE* **4000**, 2–8 (2000) [doi:doi:10.1117/12.388926].
- [13] T. A. Brunner, "Impact of lens aberrations on optical lithography," *IBM Journal of Research and Development* **41**, 57–67 (1997).
- [14] L. V. Zavyalova, B. W. Smith, T. Suganaga, S. Matsuura, T. Itani, and J. S. Cashmore, "In-situ aberration monitoring using phase wheel targets," *Proceedings of SPIE* **5377**, 172–184 (2004) [doi:doi:10.1117/12.537379].
- [15] P. Dirksen, C. A. H. Juffermans, A. Engelen, P. De Bisschop, and H. Muellerke, "Impact of high-order aberrations on the performance of the aberration monitor," *Proceedings of SPIE* **4000**, 9–17 (2000) [doi:doi:10.1117/12.389010].
- [16] B. W. Smith, W. Conley, S. Garza, J. Meute, D. A. Miller, G. K. Rich, V. L. Graffenberg, K. R. Dean, S. Patel, et al., "Aberration determination in early 157-nm exposure system," 1635–1643 (2002) [doi:10.1117/12.474551].
- [17] H. Nomura and T. Sato, "Techniques for Measuring Aberrations in Lenses Used in Photolithography with Printed Patterns," *Appl. Opt.* **38**, 2800–2807 (1999) [doi:10.1364/AO.38.002800].

DISCLAIMER

This document was prepared as an account of work sponsored by the United States Government. While this document is believed to contain correct information, neither the United States Government nor any agency thereof, nor The Regents of the University of California, nor any of their employees, makes any warranty, express or implied, or assumes any legal responsibility for the accuracy, completeness, or usefulness of any information, apparatus, product, or process disclosed, or represents that its use would not infringe privately owned rights. Reference herein to any specific commercial product, process, or service by its trade name, trademark, manufacturer, or otherwise, does not necessarily constitute or imply its endorsement, recommendation, or favoring by the United States Government or any agency thereof, or The Regents of the University of California. The views and opinions of authors expressed herein do not necessarily state or reflect those of the United States Government or any agency thereof or The Regents of the University of California.

This work was supported by the Director, Office of Science, of the U.S. Department of Energy under Contract No. DE-AC02-05CH11231.